

## On the kinematic coupling of 1D and 3D finite elements: a structural model

Jianguang Yue<sup>1\*</sup>, Apostolos Fafitis<sup>2</sup> and Jiang Qian<sup>1</sup>

<sup>1</sup>*State Key Laboratory of Disaster Reduction in Civil Engineering,  
Tongji University, Shanghai 200092, China*

<sup>2</sup>*Department of Civil and Environmental Engineering, Arizona State University,  
Tempe AZ 85287, USA*

*(Received March 3, 2010, Accepted May 19, 2010)*

**Abstract.** In most framed structures the nonlinearities and the damages are localized, extending over a limited length of the structural member. In order to capture the details of the local damage, the segments of a member that have entered the nonlinear range may need to be analyzed using the three-dimensional element (3D) model whereas the rest of the member can be analyzed using the simpler one-dimensional (1D) element model with fewer degrees of freedom. An Element-Coupling model was proposed to couple the small scale solid 3D elements with the large scale 1D beam elements. The mixed dimensional coupling is performed imposing the kinematic coupling hypothesis of the 1D model on the interfaces of the 3D model. The analysis results are compared with test results of a reinforced concrete pipe column and a structure consisting of reinforced concrete columns and a steel space truss subjected to static and dynamic loading. This structure is a reduced scale model of a direct air-cooled condenser support platform built in a thermal power plant. The reduction scale for the column as well as for the structure was 1:8. The same structures are also analyzed using 3D solid elements for the entire structure to demonstrate the validity of the Element-Coupling model. A comparison of the accuracy and the computational effort indicates that by the proposed Element-Coupling method the accuracy is almost the same but the computational effort is significantly reduced.

**Keywords:** element-coupling structural model; mixed dimensional elements; kinematic coupling; non-linear analysis.

---

### 1. Introduction

The coupling of complex systems of various scales is an important problem of structure analysis by the Finite Element and other numerical methods. One key problem is to describe the proper coupling characterization of different scales (Glimm *et al.* 1997, Wang *et al.* 2004). Barenblatt (1993) proposed a theory to solve the coupled problems, which first determine the proper transform characterization, then build a coupling equation across scales based on that characterization. For structural coupled scales, the length of the structure is a basic scale. The size of the length scale varies widely from material scale to member scale and global scale (Li *et al.* 2007). To predict the

---

\* Corresponding author, Ph.D. Student, E-mail: 79jgyue@tongji.edu.cn

structural behavior accurately at different length scales, it is fundamental to appropriately describe the coupling of those length scales. Many methods have been proposed to simulate this coupling, such as the coupling Finite Element Method (FEM) and Boundary Element Method (BEM) (Ganguly *et al.* 2000, Haas and Kuhn 2003), the coupling of FEM/FEM (McCune *et al.* 2000) and the transmit elements method (Garusi and Tralli 2002, Kim and Hong 1995).

The FEM and BEM are well-known powerful numerical techniques for solving a wide range of problems. These methods can describe the structure/member behavior at different length scales. Each method has its own advantages and disadvantages: the FEM is well suited for plastic deformation problems while the BEM allows exact satisfaction of the boundary conditions at infinity (Li *et al.* 1986). With this coupling method of FEM and BEM, the model setup is less complicated, the stress concentrations are captured more accurately in BE domains compared to FE models, and the computational effort is higher than for the FEM/FEM coupling (Haas and Kuhn 2003, Helldorfer *et al.* 2008). M. Hass gave a numerical example (a mixed dimensional 2D/3D-coupling problem of a clamped beam) to demonstrate the accuracy of the method. Using Symmetric Galerkin Boundary Element Method, FEM-like stiffness matrices can be produced which are suitable for coupling the Boundary Element Method (BEM) and the Finite Element Method. Helldorfer (2008) introduced the application of this technique used in commercial finite element systems.

In FEM, a global scale with fully 3D numerical model provides the most precise tools to capture critical details of the structural response, although its computational cost is high (Mata *et al.* 2008, Spacone and El-Tawil 2004). Moreover, a fully 1D numerical technique is rather limited to predict the mechanical behavior of structures which present local weakness that can determine their global response (Mata *et al.* 2008). Therefore, it would be desirable to combine the different dimensional elements in a single finite element model for the local damage and global behavior analysis. The mixed-dimensional FEM/FEM coupling was presented by McCune *et al.* (2000) and Shim *et al.* (2002) and further developed by Monaghan *et al.* (2000). The proper connections between beam and solid elements, and shell and solid elements could be achieved via multipoint constraint equations evaluated by equating the work done on either side of the dimensional interface. This method has been shown to give good results for coupling beam-solid elements, beam-shell elements, and shell-solid elements (Monaghan *et al.* 2000). The derivation and implementation of the corresponding weak coupling equation is a topic of current research.

The kinematic coupling is a widely-used method of coupling of FEM/FEM. The constraints imposed by kinematic coupling are usually calculated as a function of the nodal coordinates (ABAQUS 2008). This method avoids the use of multi-point constraints or Lagrange multipliers (Mata *et al.* 2008). In general, the design of the multi-point constraints requires a hypothesis about the interface stress field which is valid mainly for the simple (non-composite) materials (McCune *et al.* 2000). The Lagrange multipliers result in an increased number of variables to be determined.

Another strategy to solve the different dimensional coupling is to elaborate specific finite elements which combine the different types of elements to be connected. Kim (1995) presented three types of transition elements to solve the incompatibility related to different degrees of freedom between beam and wall elements in FE analysis. Since the transition elements can accurately model the connecting beam, the connection of coupled wall structures can be analysed effectively and reliably. Garusi (2002) presented a new transition element for modeling solid-to-beam and plate-to-beam connections, which are easily implemented and inserted in existing FE codes.

In simulating the material behavior, the classical plasticity model describes the phenomenological

behavior of the concrete failure at the macroscopic level, but cannot demonstrate the stiffness degradation caused by the micro-cracking process. The concrete plastic damage model elaborated by Lee (1998) can reflect the stiffness degradation subjected by cyclic loading at the microscopic level. Jason (2006) developed an elastic plastic damage formulation for concrete, in which the isotropic damage is responsible for the softening response and the decrease in the elastic stiffness, while hardening plasticity accounts for the development of irreversible strains and volumetric compressive behavior. Oliver *et al.* (2008) proposed a new methodology to individually identify the reinforced concrete failure as the concrete mixture theory, rebar mechanical failure, bond/slip effects and dowel action, and their relative contribution can be accounted for by using the classical mixture theory. A fiber model proposed by Cosenza *et al.* (2006) was used to simulate the existing structures where the smooth bars changed the bond mechanism.

In this paper, the focus of our research is on the Element-Coupling modeling method using the kinematic coupling technique. The Element-Coupling modeling examples of a column and a structure are given to introduce this method. The concrete plastic damage model was used to describe the local nonlinearity in the 3D model. The concrete plastic model was used to describe the global nonlinearity in the 1D model.

## 2. Element-coupling modeling strategies

### 2.1 Description of the proposed model

Structural analysis can be carried out at different length scale levels (see Fig. 1) which can be represented by different dimensional elements with different material constitutive relations. The beam elements can be at the meter level for global structural analysis or centimeter level for normal stress analysis, and solids or shell elements can be at the millimeter level for local detailed analysis.

An element-coupling model of a frame structure is shown in Fig. 1. The material scale, member scale and global scale of the structure can be determined by different analyses. The major damaged positions, such as the joints, can be determined at material scale simulated with solid elements and a complex material constitutive relation to reflect the detailed mechanical behavior. Other positions, such as beam or column members, can be determined at member scale with beam elements or shell

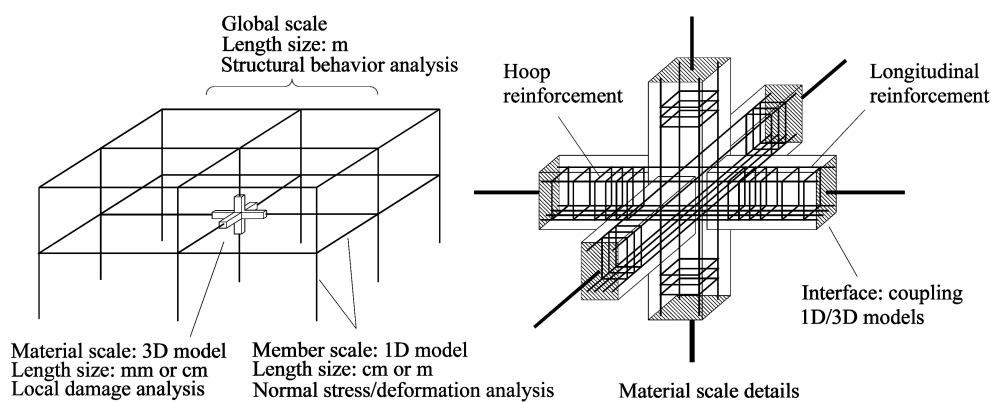


Fig. 1 Element-Coupling model

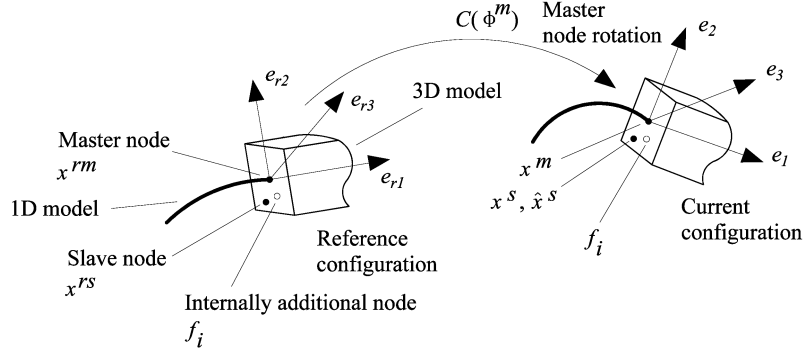


Fig. 2 Kinematic coupling of the 1D/3D models

elements and a normal material constitutive relation to reflect normal mechanical behavior. The length scale shifting can be realized by coupling mixed dimensional elements, using “kinematic coupling” or “multi-point constraint equation” methods.

## 2.2 Kinematic coupling

The dimensional-coupling between different scales is performed through interface where the kinematic coupling technique is used to consider the finite rotations and displacements. Kinematic coupling is enforced in a strict master-slave approach (see Fig. 2). Each slave node has a separate relationship with the master node. An additional node is created internally for each slave node in order to implement these constraints.

In current configuration, the position of the slave nodes can be obtained from

$$\hat{x}^s = x^m + C(\phi^m)(x^{rs} - x^{rm}) \quad (1)$$

where  $x^{rm}$  and  $x^{rs}$  are the position of the master node and slave node in the reference configuration, respectively; the superscript  $r$  denotes the reference configuration;  $\hat{x}^s$  is the fully constrained slave node position in current configuration;  $x^m$  is the position of the master node in the current configuration;  $C(\phi^m)$  is the rotation matrix associated with the master node rotation  $\phi^m$ .

The selectively constrained slave node position can be described as

$$x^s = \hat{x}^s + f_i e_i \quad (2)$$

$$e_i = C(\phi^m) \cdot e_{ri} \quad (3)$$

where  $x^s$  is the position of the slave node in the current configuration,  $f_i$  is the translation degree of freedom at the additional node,  $e_{ri}$  and  $e_i$  are the reference configuration base vectors and current configuration base vectors, respectively. Eq. (3) is independent of the choice of rotation constraint at the slave node. The release of slave node translation degree of freedom  $i$  is described as the release of translation degrees of freedom on the additional node. With these constraints on  $f_i$ , Eq. (2) can define the constraint equations.

The initial stress stiffness terms can be obtained from the second-order form of Eq. (2)

$$d(\delta x^s) = d\{\delta[x^m + C(\phi^m)(x^{rs} - x^{rm}) + f_i e_i]\} \quad (4)$$

### 2.3 Concrete plastic damage model

The “concrete plastic damage” model of ABAQUS is used to describe the nonlinear material behavior of concrete. In the plastic damage model (Lubliner *et al.* 1989), there is only one fracture-energy-based scalar damage variable used to represent all damage states. This model can simulate monotonic loading but is not appropriate for modeling cyclic loading of concrete. Lee (1998) presented a plastic damage model for cyclic loading, with two damage variables, one for tensile damage and one for compressive damage, and a yield function with multiple-hardening variables.

The strain tensor  $\boldsymbol{\varepsilon}$  is decomposed into the elastic part  $\boldsymbol{\varepsilon}^e$  and the plastic part  $\boldsymbol{\varepsilon}^p$

$$\boldsymbol{\varepsilon} = \boldsymbol{\varepsilon}^e + \boldsymbol{\varepsilon}^p; \quad \boldsymbol{\varepsilon}^e = \mathbf{E}^{-1} : \boldsymbol{\sigma} \quad (5a, b)$$

where  $\mathbf{E}$  is the elastic stiffness tensor,  $\boldsymbol{\sigma}$  is the stress tensor.

The plastic strain represents all irreversible deformations including those caused by microcracks. From Eq. (5) the stress-strain relation is

$$\boldsymbol{\sigma} = \mathbf{E} : (\boldsymbol{\varepsilon} - \boldsymbol{\varepsilon}^p) \quad (6)$$

From the concept of the continuum damage theory, the stress is mapped into the effective stress  $\bar{\boldsymbol{\sigma}}$  by a rank four tensor  $\mathbf{D}$

$$\bar{\boldsymbol{\sigma}} = \mathbf{D} : \boldsymbol{\sigma} \quad (7)$$

A scalar degradation damage variable  $0 \leq D < 1$  is used to represent the isotropic damage, then  $\mathbf{D} = 1 / (1 - D) \mathbf{I}$ , where  $\mathbf{I}$  is the rank four identity tensor, and the effective stress is

$$\bar{\boldsymbol{\sigma}} = (1 - D) \mathbf{E}_0 : (\boldsymbol{\varepsilon} - \boldsymbol{\varepsilon}^p) \quad (8)$$

where  $\mathbf{E}_0$  is the initial elastic-stiffness tensor,  $D$  represents the degradation of the elastic stiffness.

The plastic strain rate  $\dot{\boldsymbol{\varepsilon}}^p$  is evaluated by a flow rule, which is assumed to be generated from a scalar plastic potential function  $\Phi$

$$\dot{\boldsymbol{\varepsilon}}^p = \dot{\lambda} \nabla_{\boldsymbol{\sigma}} \Phi(\bar{\boldsymbol{\sigma}}) \quad (9)$$

where  $\dot{\lambda}$  is a nonnegative function referred to as the plastic consistency parameter.

The damage variable  $\kappa$  is defined using  $\kappa_t$  and  $\kappa_c$ , which are independent state variables. The evolution is expressed as

$$\dot{\kappa} = \dot{\lambda} H(\bar{\boldsymbol{\sigma}}, \kappa) \quad (10)$$

where  $\dot{\lambda}$  is a nonnegative function referred to as the plastic consistency parameter, the function  $H$  can be derived considering plastic dissipation.

The total stress  $\boldsymbol{\sigma}$  is determined by evaluating the degradation damage from

$$\boldsymbol{\sigma} = [1 - D(\kappa)] \bar{\boldsymbol{\sigma}} \quad (11)$$

where the degradation damage variable  $D$  is defined as  $D = D(\kappa) = 1 - (1 - d_t)(1 - d_c)$ , which describes tensile  $d_t$  and compressive  $d_c$  degradation damage responses. More details of the concrete plastic damage can be found in Lee (1998) and ABAQUS Theory Manual (2008).

The compressive damage variable and tensile damage variable are written as (Birtel and Mark 2006)

$$d_c = 1 - \frac{\sigma_c E_c^{-1}}{\varepsilon_c^{pl} (1/b_c - 1) + \sigma_c E_c^{-1}} \quad (12a)$$

$$d_t = 1 - \frac{\sigma_t E_t^{-1}}{\varepsilon_t^{pl} (1/b_t - 1) + \sigma_t E_t^{-1}} \quad (12b)$$

where  $b_c$  is equal to 0.7 and  $b_t$  is equal to 0.1.

The concrete model proposed by Desayi and Krishnan (1964) is used for the uniaxial compressive stress-strain curve in this study

$$\sigma = E_c \varepsilon / (1 + (\varepsilon / \varepsilon_0)^2) \quad (13)$$

where  $\varepsilon_0$  is the strain corresponding to the peak stress,  $\varepsilon_0 = 2f_c' / E_c$ ,  $E_c$  is the concrete initial elastic modulus,  $f_c'$  is the concrete cylinder strength. The limited compressive strain  $\varepsilon_u$  is assumed as 0.0035.

By direct stress-crack strain curve, the concrete tensile stress-strain curve reflects the tensile softening and is assumed as linear before tensile peak stress. After peak stress, the tensile stress-strain curve is given as follows (Cornelissen and Reinhardt 1984)

$$\frac{\sigma}{f_t} = \left[ 1 + c_1 \left( \frac{\varepsilon}{\varepsilon_{tu}} \right)^4 \right] e^{-c_2 \frac{\varepsilon}{\varepsilon_{tu}}} \quad (14)$$

where  $f_t$  is concrete tensile strength,  $\varepsilon_{tu}$  is concrete limited tensile strain, here it is equal to 0.001,  $c_1$  and  $c_2$  are equal to 9.0 and 5.0, respectively.

### 3. Modeling of a structural member

Tu (2006) and Rong (2006) had done a quasi-static test of a reinforced concrete pipe column (see Fig. 3). The column test model details are shown in Fig. 4. The compressive strength of the



Fig. 3 Column test model

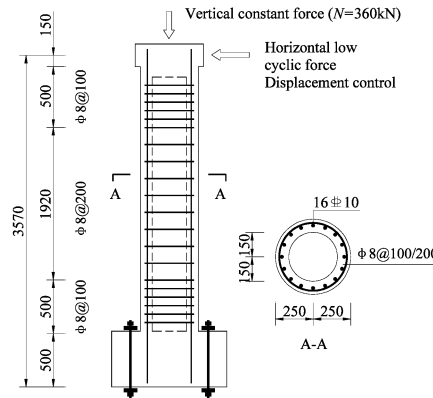


Fig. 4 Column test details (unit: mm)



Fig. 5 Column damage

concrete is 42.0 MPa. At the top of the column, a constant vertical force of 360 kN was applied vertically while a gradually increasing force was applied horizontally through controlling the top displacement. As the top displacement was increasing, cracks developed at the bottom of the column, and the concrete at the bottom failed (see Fig. 5).

### 3.1 Calculation model

This test is simulated by two different finite element models, which are named model 1 and model 2. Here, the longitudinal and hoop reinforcements are assumed as ideally elastic-plastic with yielding stress of 360 MPa and 210 MPa, respectively. The plastic model and the plastic damage model (mentioned in section 2.3) were used in the 1D and 3D elements to describe the concrete nonlinear behavior, respectively.

#### 3.1.1 Model 1 – Full-3D-Element model

In general, a pure three dimensional element model will reflect accurately the column behavior

and it will serve as reference. The concrete and reinforcement of the column are simulated by the C3D8R elements and T3D2 elements. C3D8R is an 8-node linear brick continuum element with reduced integration by hourglass control. T3D2 is a 3D stress/displacement 2-node linear displacement truss element of ABAQUS software. The reinforcement elements are embedded in the concrete elements. The elements embedded technique is used to specify an element or a group of elements that lie embedded in a group of host elements whose response will be used to constrain the translational degrees of freedom of the embedded nodes.

### 3.1.2 Model 2 – Element-Coupling model

Within the region from the column bottom to a height of 750 mm, the simulations of the concrete and reinforcement are the same with the Model 1. In the other region, the concrete is simulated with B31 elements. B31 is a Timoshenko 2-node linear beam element in space. The 3D elements and 1D element are coupled by the kinematic coupling technique of ABAQUS.

## 3.2 Calculation results

Fig. 6 shows the experimental load-displacement curves and the curves obtained by the two finite element models. The calculation results of Model 1 and Model 2 are very similar, but the result of test shows some variation. The limit load of the test is 67.4 kN (Tu 2006, Rong 2006), the calculated limit loads of Model 1 and Model 2 are 61.7 kN and 61.1 kN, respectively. Those results indicate that the two finite element models can reflect the column behavior well at the member scale.

For studying the material damage, the local simulation accuracy of the Element-Coupling model is verified by comparing the max equivalent plastic strain of concrete and the von Mises stress of reinforcement in the two finite elements models. The equivalent plastic strain gives a measure of the amount of permanent strain in an engineering body and it is calculated from the component plastic strain. Equivalent plastic strain is defined as  $\bar{\varepsilon}^p = \int \dot{\varepsilon}^p dt$ , where  $\dot{\varepsilon}^p$  is the equivalent plastic strain rate. Fig. 7 shows the relation of the column top displacements and concrete max equivalent plastic strain. The max equivalent plastic strain of Model 1 and Model 2 are 0.013 and 0.010, respectively. Furthermore, the behavior of the steel can be studied by extracting the von Mises stress results from a steel element node. Fig. 8 shows the results of reinforcement von Mises stress in the two finite

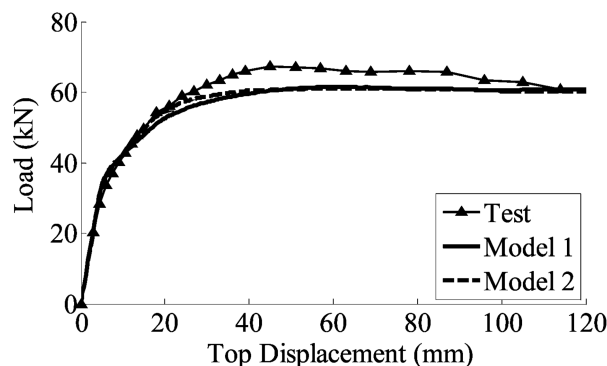


Fig. 6 Comparison of the load-displacement curves

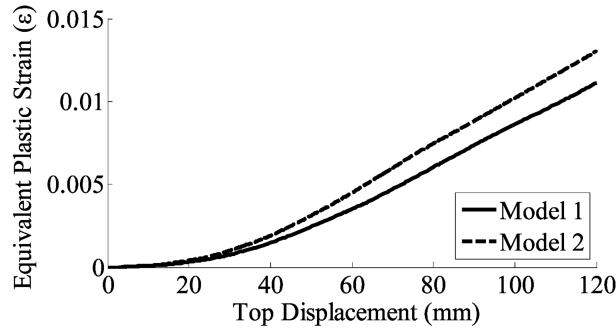


Fig. 7 Top displacement-equivalent plastic strain curves

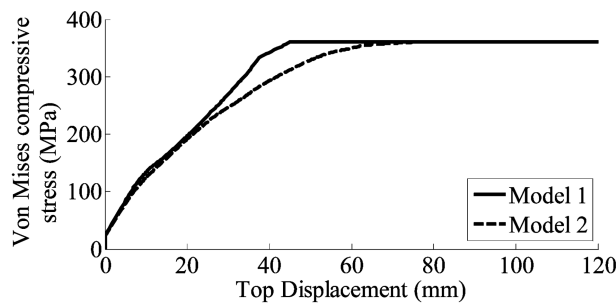


Fig. 8 Top displacement-von Mises stress curves

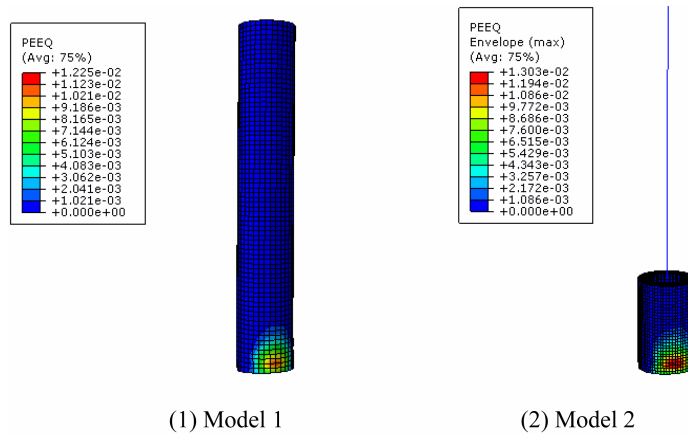


Fig. 9 Comparison of the concrete max PEEQ

element models. The reinforcement of Model 1 and Model 2 yielded at the top displacements of 45 mm and 75 mm, respectively.

Those results indicate that the Element-Coupling model has a similar local simulation with the solid column model.

Fig. 9 shows the contours of concrete max equivalent plastic strain of the two models. Fig. 10

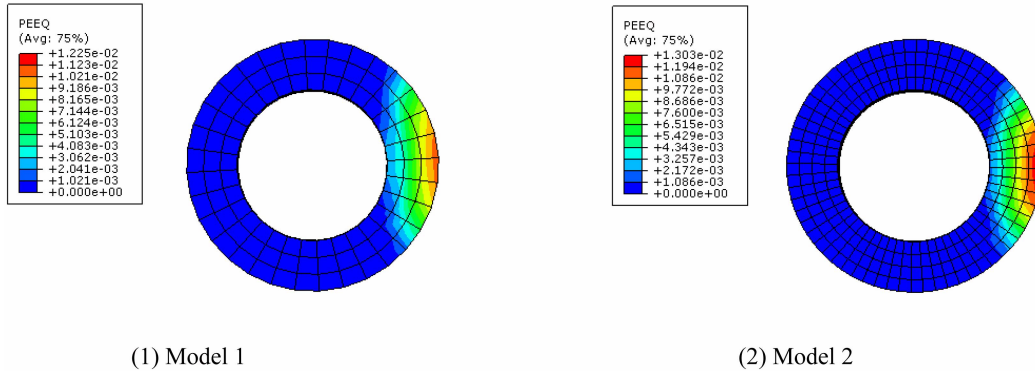


Fig. 10 Comparison of the concrete max PEEQ of the column section

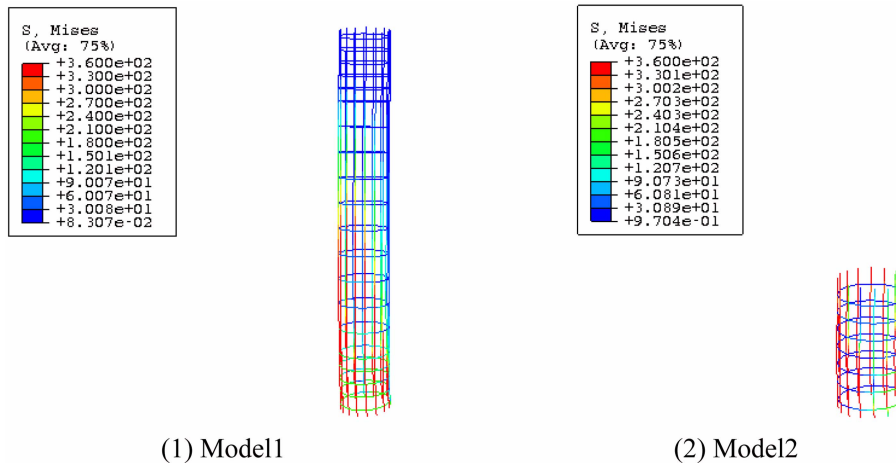


Fig. 11 Comparison of the reinforcement von Mises stress (unit: MPa)

shows the contours of cross section strain distribution of the two models. PEEQ denotes the equivalent plastic strain in uniaxial compression. The cross sections of Fig. 10 were at the bottom of the columns in Model 1 and Model 2, respectively.

Fig. 11 shows the reinforcement von Mises stress of the two models. The cross section strain distribution of Model 2 is similar to Model 1. And Model 1 can reflect the failures accurately. The focus of Model 2 is at the bottom of the column where the major damage took place. In those contour pictures, the “Avg: 75%” denotes averaging threshold at 75%.

The CPU calculation times of Model 1 and Model 2 are 4851 seconds and 786 seconds, respectively. The computational efficiency of Model 2 is approximately six times to Model 1.

#### 4. Modeling of the structure

Bai *et al.* (2008) have conducted pseudo-static and pseudo-dynamic model tests of a substructure



Fig. 12 A direct air-cooled condenser support platform



Fig. 13 Test model and loading transfer device

from a direct air-cooled condenser support platform (see Fig. 12). This test is to study the dynamic performance of the platform. The platform is a vertical hybrid structure consisting of reinforced concrete pipe columns and steel truss. The pipe column height is about 40 m, its section diameter is about 4m and its thickness is about 0.5 m. The steel truss height is about 8 m. The total weight of the equipments on the platform is more than 10 thousand tons. The reduction scale of the test model (see Fig. 13) is 1:8 for the overall dimensions of the structure as well as the dimension of the members (columns and truss). More information can be found in Li (2006).

In the test model, the measured value of concrete compressive strength is 26.64 MPa, the strength grades of longitudinal and hoop reinforcements are HRB400 (yielding stress 400 MPa) and HRB235 (yielding stress 235 MPa) (GB50010-2002), respectively. The truss is made of square steel tubular members, and the major sections are  $60 \times 2.5 \text{ mm}^2$ ,  $60 \times 2.0 \text{ mm}^2$ ,  $50 \times 1.5 \text{ mm}^2$  and  $25 \times 1.5 \text{ mm}^2$ . The steel strength grade is Q235 (yielding stress equal to 235 MPa) (GB50017-2003). The pipe column had an external radius of 250 mm and a wall thickness of 50 mm. The pipe column was reinforced with 15 bars of longitudinal reinforcements (diameter 10 mm) and hoop reinforcements (diameter 8 mm) with spacings of 100 mm at the bottom section and 200 mm elsewhere. The plane and profile drawings of the test model are shown in Fig. 14.

Two hydraulic-servo actuators (see Fig. 13) were used to apply the loads on the structure through the loading transfer device, which will transfer the loads from the hydraulic servo-actuator to 14 loading points of the structure (see Figs. 13 and 14). Displacement gauges were used to measure the

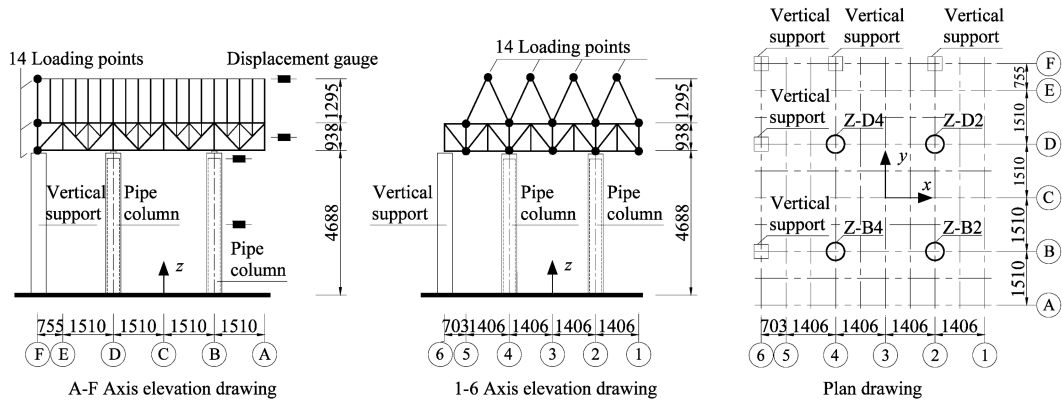
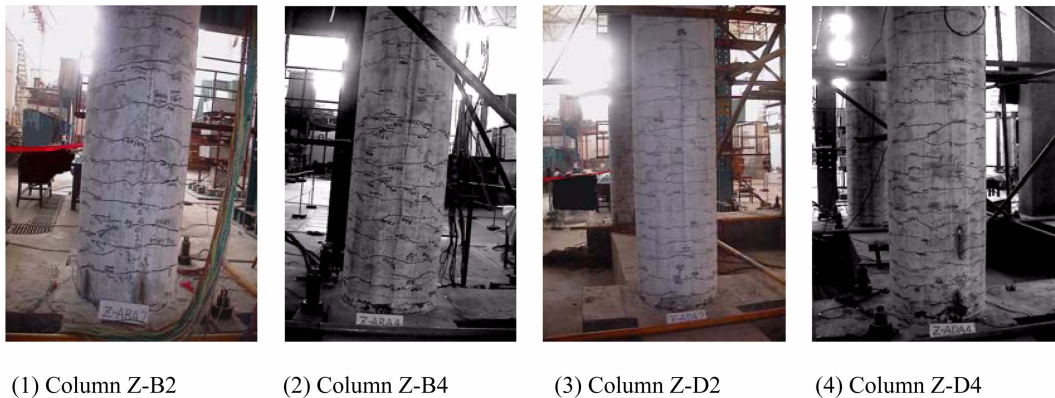


Fig. 14 Plane and profile drawing of the test model (unit: mm)



(1) Column Z-B2

(2) Column Z-B4

(3) Column Z-D2

(4) Column Z-D4

Fig. 15 Columns damage of the test model

structure top displacement, the truss displacement, the column top displacement and the column middle displacement (see Fig. 14).

In the pseudo-dynamic test, El Centro (1940 NS) wave was the input at the loading points, with peak accelerations  $50 \text{ cm/sec}^2$ ,  $100 \text{ cm/sec}^2$ ,  $200 \text{ cm/sec}^2$ ,  $400 \text{ cm/sec}^2$ ,  $600 \text{ cm/sec}^2$  and  $800 \text{ cm/sec}^2$ . According to the similarity principle, the time interval should be adjusted to  $\Delta t / \sqrt{8}$ . The structural damping ratio is about 3.5 percent of critical damping under  $50 \text{ cm/sec}^2$  peak acceleration, 8 percent under  $100 \text{ cm/sec}^2$  peak acceleration, and 1.2 percent under  $200 \text{ cm/sec}^2$ ,  $400 \text{ cm/sec}^2$ ,  $600 \text{ cm/sec}^2$  and  $800 \text{ cm/sec}^2$  peak acceleration. When the peak accelerations were  $50 \text{ cm/sec}^2$ ,  $100 \text{ cm/sec}^2$ , and  $200 \text{ cm/sec}^2$ , the structural behavior was linearly elastic; when the peak acceleration was  $400 \text{ cm/sec}^2$ , some horizontal cracks occurred in the column bottom; when the peak acceleration was  $600 \text{ cm/sec}^2$ , much more cracks occurred; when the peak acceleration reached  $800 \text{ cm/sec}^2$ , the concrete failed at the bottom of the column, while most longitudinal reinforcement and some hoop reinforcement yielded.

In the pseudo-static test, the test loading was controlled by the top displacement. When the top displacement reached 110 mm, the concrete failed at the column bottom (see Fig. 15). Truss failure occurred mostly in the joint zone near the top of the columns.

#### 4.1 Calculation model

The test is simulated by two finite element models. The reinforcement is assumed elastic-plastic. The yielding stresses of longitudinal reinforcement and hoop reinforcement were 360 MPa and 210 MPa, respectively. The structural steel is also assumed elastic-plastic with yielding stress equal to 215 MPa. The density of the steel is  $7.9 \text{ g/cm}^3$ . The plastic model and the plastic damage model (mentioned in section 2.3) were used in the 1D and 3D elements to describe the concrete nonlinear behavior. The concrete cubic compressive strength was 26.64 MPa. The average mass density of concrete was  $2.4 \text{ g/cm}^3$ .

##### 4.1.1 Model 1 – Full-3D-Elements model

A finite element model in which the columns are solid elements is built for reference. The truss was simulated with B31 elements of ABAQUS; the concrete slab on the truss was simulated with S4R elements. S4R is a 4-node, quadrilateral, stress/displacement shell element with reduced integration and a large-strain formulation. The concrete and reinforcement of the column were simulated with C3D8R elements and T3D2 elements, and the bar elements were embedded in the concrete elements.

##### 4.1.2 Model 2 – Element-Coupling model

The truss was simulated with B31 elements of ABAQUS. Concrete and reinforcement in the region from column bottom to the height of 1100 mm were simulated with C3D8R elements and T3D2 elements of ABAQUS, and the bar elements were embedded in the concrete elements. Concrete in the other region was simulated with the B31 elements without the reinforcement. The coupling of the different concrete elements was realized by the kinematic coupling technique of ABAQUS.

#### 4.2 Dynamic calculation results

The fundamental frequencies computed by the two models are compared with the experiment results in Table 1.

As shown in Figs. 16 and 17, the first two modal shapes of the two models indicate that the model reflects the dynamic properties well.

In the dynamic analysis, an automatic incremental scheme is used with the general implicit dynamic integration method. The computed top displacement and base shear are compared with the experiment results in Table 2. The agreement is satisfactory.

The concrete max equivalent plastic strains in column and the reinforcement max von Mises stress computed by the two models are compared in Table 3. The agreement is satisfactory.

Under the peak acceleration of  $800 \text{ cm/sec}^2$  waves, the column concrete max equivalent plastic

Table 1 Comparison of the dynamic properties

Mode	Measured frequency (Hz)	Model 1		Model 2	
		frequency (Hz)	Modal shape	frequency (Hz)	Modal shape
1	3.20	3.06	Torsion	3.17	Torsion
2	4.59	3.43	y-Translation	3.43	y-Translation

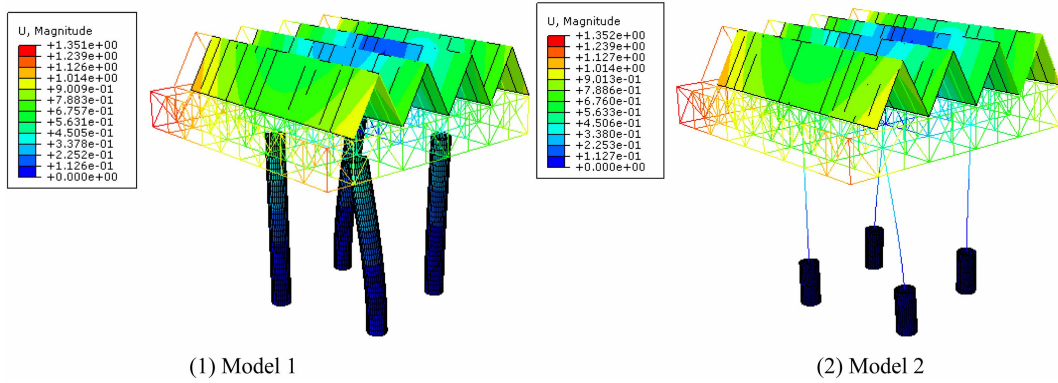


Fig. 16 Modal shape of the first order

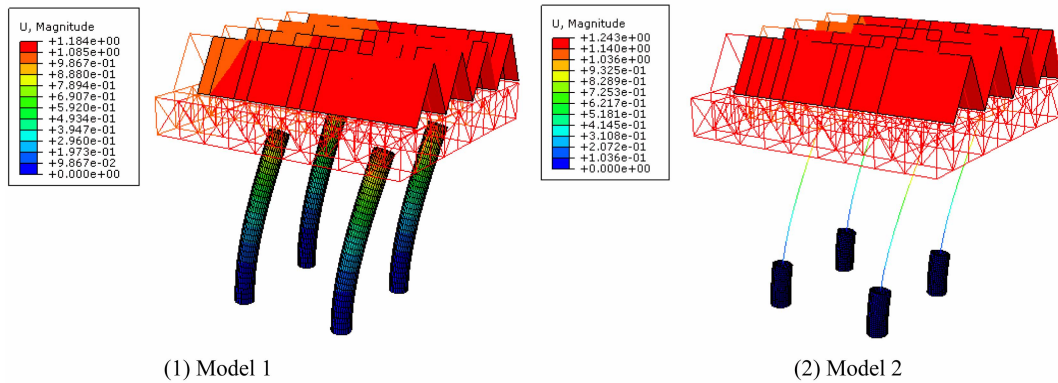


Fig. 17 Modal shape of the second order

Table 2 Comparison of the top displacement and the base shear of the structure

Peak acceleration (cm/sec <sup>2</sup> )	Top displacement (mm)			Base shear (kN)		
	Test	Model 1	Model 2	Test	Model 1	Model 2
50	1.73	1.49	1.40	11.55	10.94	8.27
100	2.20	2.89	2.80	16.36	18.25	15.70
200	4.93	5.68	5.60	29.33	29.73	24.08
400	16.80	16.73	17.26	48.04	53.53	50.47
600	22.20	25.04	24.83	65.57	72.11	69.21
800	33.23	33.36	34.00	102.2	92.47	90.17

strain vs the structure top displacement and the reinforcement max stress vs the structure top displacement are shown in Figs. 18 and 19, respectively.

Under the peak acceleration of 800 cm/sec<sup>2</sup> waves, the concrete max equivalent plastic strains are shown in Fig. 20. The column cross section concrete max equivalent plastic strain distributions are

Table 3 Comparison of the concrete max equivalent plastic strain and the reinforcement max von Mises stress

Peak acceleration (cm/sec <sup>2</sup> )	Concrete max equivalent plastic strain ( $\mu\epsilon$ )		Reinforcement max Mises stress (MPa)	
	Model 1	Model 2	Model 1	Model 2
50	0	0	10.3	8.2
100	0	0	20.9	18.4
200	0	0	48.0	52.9
400	33.6	25.5	198.0	212.3
600	133.2	115.7	269.9	309.1
800	258.2	277.7	341.3	360.0

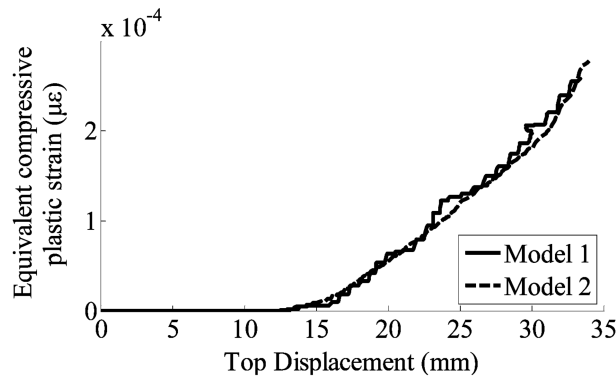


Fig. 18 Top displacement-equivalent plastic strain curves

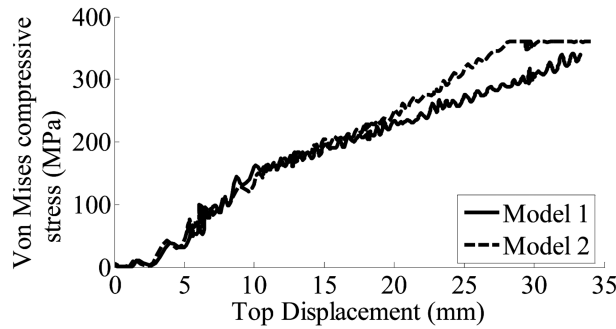


Fig. 19 Top displacement-von Mises stress curves

shown in Fig. 21. The reinforcement and the truss max stress of the two models are shown in Fig. 22. In Fig. 21, the cross sections were at the bottom of the column Z-B4.

Most of the concrete damage is at the bottom of the column. The longitudinal bars and the hoop bars also yielded at the bottom of the columns. The truss failures occurred mostly in the region near the top of the columns. The cross section strain distribution of Model 2 is similar to Model 1. Model 1 predicts the failures completely and Model 2 reflects the major failures.

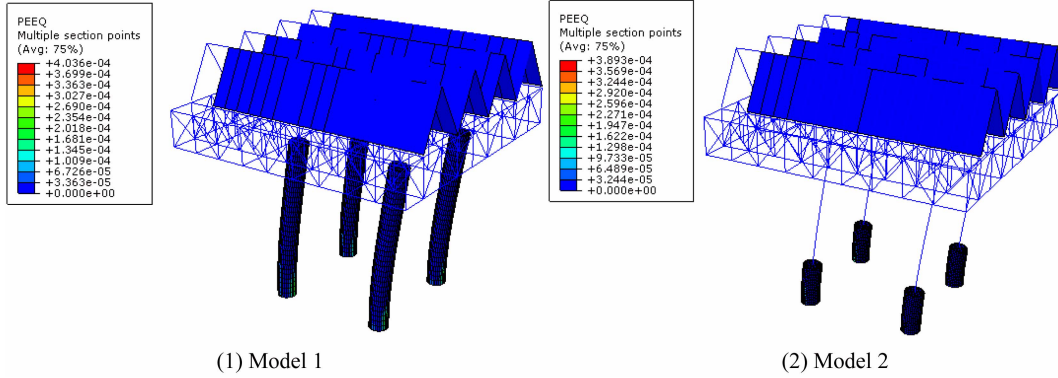


Fig. 20 Comparison of the concrete max PEEQ

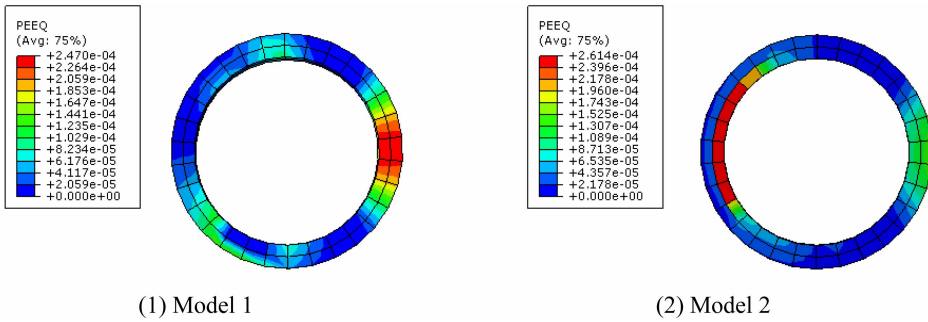


Fig. 21 Comparison of the concrete max PEEQ of the column section

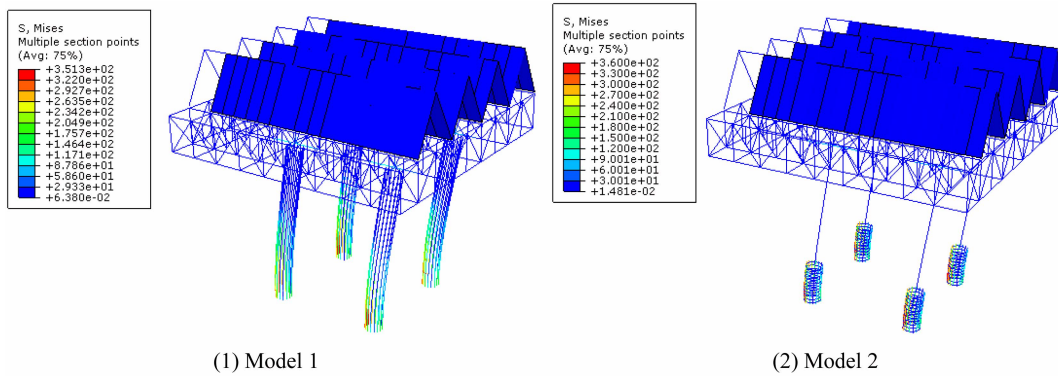


Fig. 22 Comparison of the max Von Mises stress of the reinforcement and truss (unit: MPa)

Table 4 shows the CPU calculation time for the two finite element models. In the linear stage, the computational efficiency of Model 2 is approximately four times faster than that of Model 1; in the nonlinear stage, the computational efficiency of Model 2 is approximately ten times faster than that of Model 1.

Table 4 Dynamic calculation efficiency comparison

Peak acceleration (cm/sec <sup>2</sup> )		50	100	200	400	600	800
CPU Time (second)	Model 1	2367	2500	4257	13801	21976	27713
	Model 2	571	751	790	1501	1636	2120

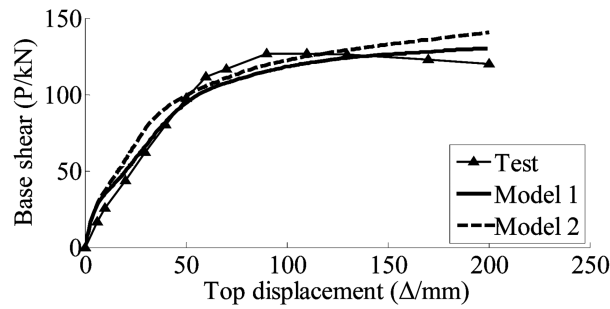


Fig. 23 Comparison of the load-displacement curves

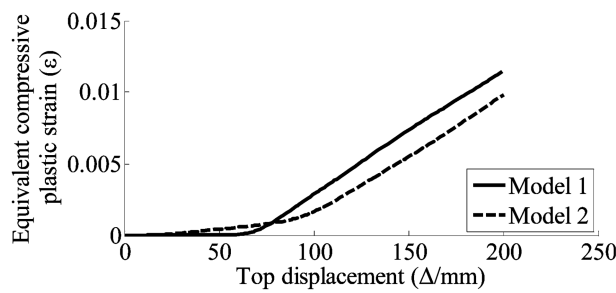


Fig. 24 Top displacement-equivalent plastic strain curves

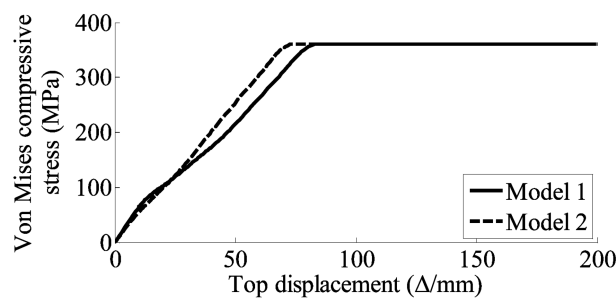


Fig. 25 Top displacement-von Mises stress curves

### 4.3 Static calculation results

The load-displacement curves of the two models and the test are shown in Fig. 23.

The concrete max equivalent plastic strains and max reinforcement stresses in the two models are compared in Fig. 24 and 25 respectively, which indicate that the model predicts a similar local

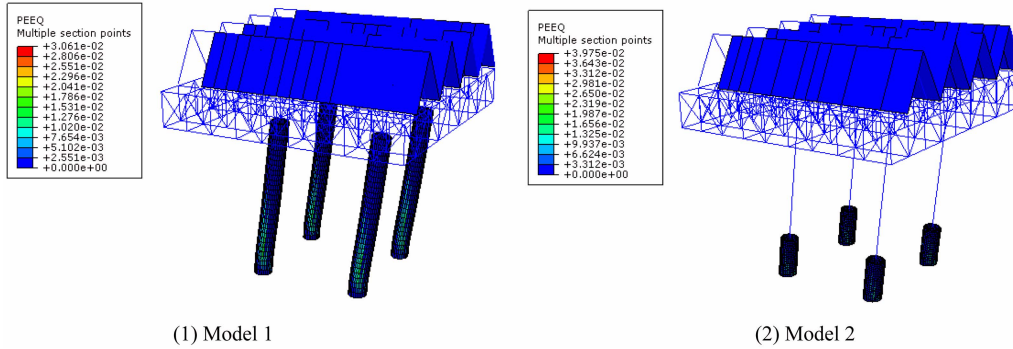


Fig. 26 Comparison of the concrete max equivalent plastic strain

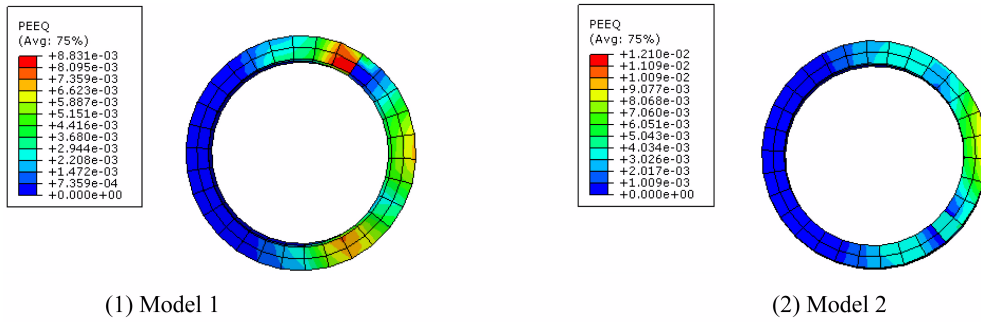


Fig. 27 Comparison of the concrete max PEEQ of the column section

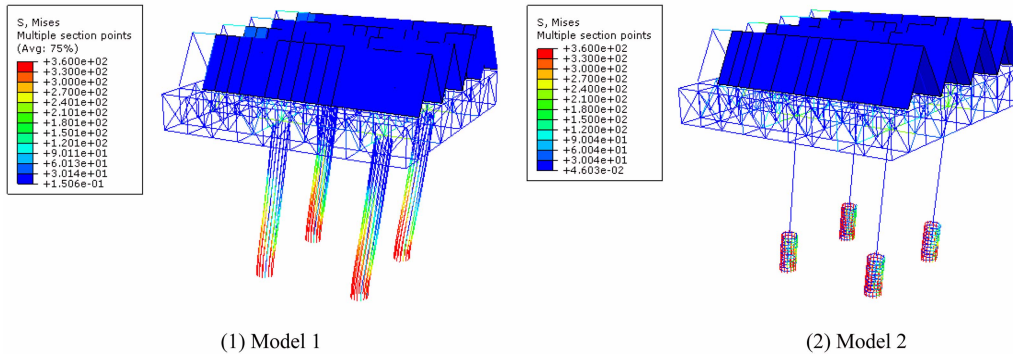


Fig. 28 Comparison of the max Von Mises stress of the reinforcement and truss (unit: MPa)

behavior with the solid column model. Although the overall behavior predicted by the models agrees with the experimental data, the models do not capture the slight softening behavior of the test specimen.

The results of concrete max equivalent plastic strain, column cross section concrete max equivalent plastic strain distribution, and reinforcement and truss Mises stress are shown in Figs. 26, 27 and 28, respectively. In Fig. 27, the cross sections were at the bottom of the column Z-B4 in Model 1 and Model 2. Those static calculated results indicate that the model simulates the overall

structural behavior and the local behavior well.

The CPU calculation times of Model 1 and Model 2 are 2940 seconds and 152 seconds, respectively. The computational effort of Model 2 is significantly reduced.

## 5. Conclusions

An Element-Coupling model is studied in this paper using the kinematic coupling technique with ABAQUS software. The concrete local damage can be reflected by the 3D models with the concrete plastic damage model. The validity of the method is demonstrated by comparing the results of nonlinear analysis with test results of a reinforced concrete pipe column and a composited structure subjected to static and dynamic loadings.

Under static and dynamic actions, the Element-Coupling models of member and structure reflect well the behavior in the member scale and the structure scale, and predict major failure areas as well as local failures in the material scale, which are in good agreement with the test results.

The Element-Coupling model has a superior computational efficiency.

## Acknowledgements

Financial supports from the National Basic Research Program of China (Grant No. 2007CB714202) and from China Scholarship Council are gratefully acknowledged. The authors particularly wish to thank Prof. G. L. Bai (Xi'an University of Architecture and Technology) for his help to provide the test results.

## References

- ABAQUS Theory Manual (2008), "Version 6.8", ABAQUS Inc., USA.
- Bai, G.L., Zhu, L.H., Zhao, C.L., Li, H.X. and Li, X.W. (2008), "Model test on behavior of direct air cooled condenser support platform under load and earthquake action", *J. Build. Struct.*, **29**(5), 42-49.
- Barenblatt, G.I. (1993), *Micromerchanics of fracture*, Theoretical and Applied Mechanics, Elsevier Science Publishers B.V., 25-52.
- Birtel, V. and Mark, P. (2006), "Parameterised finite element modeling of RC beam shear failure", ABAQUS User's Conference, 95-107.
- Cornelissen, H.A.W. and Reinhardt H.W. (1984), "Uniaxial tensile fatigue failure of concrete under constant-amplitude and program loading", *Mag. Concrete Res.*, **36**(129), 216-226.
- Cosenza, E., Manfredi, G. and Verderame, G.M. (2006), "A fibre model for push-over analysis of underdesigned reinforced concrete frames", *Comput. Struct.*, **84**(13-14), 904-916.
- Desayi, P. and Krishnan, S. (1964), "Equation for the stress-strain curve of concrete", *J. Am. Concrete Institute*, **61**, 345-350.
- Ganguly, S., Layton, J.B. and Balakrishna, C. (2000), "Symmetric coupling of multi-zone curved Galerkin boundary elements with finite elements in elasticity", *Int. J. Numer. Method. Eng.*, **48**, 663-654.
- Garusi, E. and Tralli, A. (2002), "A hybrid stress-assumed transition element for solid-to-beam and plate-to-beam connections", *Comput. Struct.*, **80**(2), 105-115.
- GB50010-2002 (2002), *Code for design of concrete structures*, China Architecture and Building Press, Beijing.
- GB50017-2003 (2003), *Code for design of steel structures*, China Architecture and Building Press, Beijing.

- Glimm, J. and Sharp, D. (1997), "Multiscale science: a challenge for the twenty-first century", *SIAM News* **30**(8), 1-7.
- Haas, M. and Kuhn, G. (2003), "Mixed-dimensional, symmetric coupling of FEM and BEM", *Eng. Anal. Bound. Elem.*, **27**(6), 575-582.
- Helldorfer, B., Haas, M. and Kuhn, G. (2008), "Automatic coupling of a boundary element code with a commercial finite element system", *Adv. Eng. Softw.*, **39**(8), 699-709.
- Jason, L., Huerta, A., Pijaudier-Cabot, G. and Ghavamian, S. (2006), "An elastic plastic damage formulation for concrete: application to elementary tests and comparison with an isotropic damage model", *Comput. Method. Appl. M.*, **195**(52), 7077-7092.
- Kim, H.S. and Hong, S.M. (1995), "Formulation of transition-elements for the analysis of coupled wall structures", *Comput. Struct.*, **57**(2), 333-344.
- Lee, J.H. and Fenves, G.L. (1998), "Plastic-damage model for cyclic loading of concrete structures", *J. Eng. Mech. - ASCE*, **124**(8), 892-900.
- Li, H.B., Han, G.M., Mang, H.A. and Torzicky, P. (1986), "A new method for the coupling of finite-element and boundary element discretized subdomains of elastic bodies", *Comput. Method. Appl. M.*, **54**(2), 161-185.
- Li, H.X. (2006), "Study on the support system for air cooled condenser of big power plant", Ph.D. Thesis, Xi'an University of Architecture and Technology, Xi'an.
- Li, Z.X., Zhou, T.Q., Chan, T.H.T. and Yu, Y. (2007), "Multi-scale numerical analysis on dynamic response and local damage in long-span bridges", *Eng. Struct.*, **29**(7), 1507-1524.
- Lublinter, J., Oliver, J., Oller, S. and Onate, E. (1989), "A plastic-damage model for concrete", *Int. J. Solids Struct.*, **25**(3), 299-326.
- Mata, P., Barbat, A.H. and Oller, S. (2008), "Two-scale approach for the nonlinear dynamic analysis of RC structures with local non-prismatic parts", *Eng. Struct.*, **30**(12), 3667-3680.
- McCune, R.W., Armstrong, C.G. and Robinson, D.J. (2000), "Mixed-dimensional coupling in finite element models", *Int. J. Numer. Method. Eng.*, **49**(6), 725-750.
- Monaghan, D.J., Lee, K.Y., Armstrong, C.G. and Ou, H. (2000), "Mixed dimensional finite element analysis of frame models", *10th ISOP Conference*, Seattle, 263-269.
- Oliver, J., Linero, D.L., Huespe, A.E. and Manzoli, O.L. (2008), "Two-dimensional modeling of material failure in reinforced concrete by means of a continuum strong discontinuity approach", *Comput. Method. Appl. M.*, **197**(5), 332-348.
- Rong, Z. (2006), "An experimental research on seismic behavior of great size thin wall reinforced concrete columns", M.D. Thesis, Xi'an University of Architecture and Technology, Xi'an.
- Shim, K.W., Monaghan, D.J. and Armstrong, C.G. (2002), "Mixed dimensional coupling in finite element stress analysis", *Eng. Comput.*, **18**(3), 241-252.
- Spacone, E. and El-Tawil, S. (2004), "Nonlinear analysis of steel-concrete composite structures: state of the art", *J. Struct. Eng. - ASCE*, **130**(2), 159-168.
- Tu, F. (2006), "Experimental study and nonlinear finite analysis on seismic behavior of reinforced concrete pipe columns with large size and thin wall", M.D. Thesis, Xi'an University of Architecture and Technology, Xi'an.
- Wang, H.Y., He, G.W., Xia, M.F., Ke, F.J. and Bai, Y.L. (2004), "Multiscale coupling in complex mechanical systems", *Chem. Eng. Sci.*, **59**(8-9), 1677-1686.